Lifetime measurements in ^{100}Ru

T. Konstantinopoulos,[1] P. Petkov,[2,3,*] A. Goasduff,[1,4] T. Arici,[5] A. Astier,[1] L. Atanasova,[6] M. Axiotis,[7] D. Bonatsos,[7] P. Detistov,[3] A. Dewald,[8] M. J. Eller,[9,†] V. Foteinou,[7] A. Gargano,[10] G. Georgiev,[1] K. Gladnishki,[11] A. Gottardo,[9] S. Harissopulos,[7] H. Hess,[8] S. Kaim,[1,‡] D. Kocheva,[11] A. Kusoglu,[1,12] A. Lagoyannis,[7] J. Ljungvall,[1] R. Lutter,[13] I. Matea,[9] B. Melon,[14] T. J. Mertzimekis,[15] A. Nannini,[14] C. M. Petrache,[1] A. Petrovici,[2] G. Provatas,[7] P. Reiter,[8] M. Rocchini,[14] S. Roccia,[1] M. Seidlitz,[8] B. Siebeck,[8] D. Suzuki,[9,§] N. Warr,[8] H. De Witte,[16] and T. Zerrouki[1]

[1]*CSNSM, Université Paris-Sud, CNRS/IN2P3, Université Paris-Saclay, 91405 Orsay, France*

[2]*National Institute for Physics and Nuclear Engineering - Horia Hulubei, R-077125 Bucharest, Romania*

[3]*INRNE, Bulgarian Academy of Sciences, 1784 Sofia, Bulgaria*

[4]*Istituto Nazionale di Fisica Nucleare, Laboratori Nazionali di Legnaro, I-35020 Legnaro, Italy*

[5]*Helmholtzzentrum für Schwerionenforschung GmbH (GSI), Darmstadt, Germany*

[6]*Department of Medical Physics and Biophysics, Medical University - Sofia, 1431, Sofia, Bulgaria*

[7]*TANDEM Accelerator Laboratory, Institute of Nuclear Physics, NCSR "Demokritos", 15310 Aghia Paraskevi, Athens, Greece*

[8]*Institut für Kernphysik, Universität zu Köln, Zülpicherstr. 77, 50937 Köln, Germany*

[9]*INP, Université Paris-Sud, CNRS/IN2P3, Université Paris-Saclay, 91405 Orsay, France*

[10]*Istituto Nazionale di Fisica Nucleare, Complesso Universitario di Monte S. Angelo, Via Cintia, I-80126 Napoli, Italy*

[11]*University of Sofia, Sofia, Bulgaria*

[12]*Department of Physics, Faculty of Science, Istanbul University, Vezneciler/Fatih, 34134 Istanbul, Turkey*

[13]*Fakultät für Physik, Ludwig-Maximilians-Universität München, D-85748 Garching, Germany*

[14]*INFN Sezione di Firenze, I-50019 Firenze, Italy*

[15]*Department of Physics, University of Athens, Zografou Campus, GR-15784 Athens, Greece*

[16]*KU Leuven, Instituut voor Kern- en Stralingsfysica, 3001 Leuven, Belgium*

(Received 1 December 2016; published 10 January 2017)

The nucleus ^{100}Ru appears to be a good candidate for the E(5) critical point symmetry which describes the U(5)-SO(6) shape phase transition. To investigate this point with respect to the electromagnetic transition strengths, lifetime measurements of its yrast states have been performed using the recoil distance Doppler shift technique as well as the Doppler shift attenuation method. As a result, the lifetimes of the yrast 2^+, 4^+, and 8^+ states were determined. The deduced transition strengths are compared to the E(5) predictions as well as to the results of excited Vampir and shell-model calculations.

DOI: 10.1103/PhysRevC.95.014309

I. INTRODUCTION AND MOTIVATION

It has been 15 years since the critical point symmetries E(5) [1] and X(5) [2] were introduced by Iachello. These symmetries describe nuclei that are close to the critical point of the shape phase transition U(5)-SO(6) for the former and U(5)-SU(3) for the latter. In particular, they provide excitation energies and transition probabilities which can be directly compared to the experiment within overall scaling factors.

Based on these predictions, the best realization of the E(5) critical point symmetry was found so far in the nucleus ^{134}Ba [3]. Other nuclei such as ^{104}Ru, ^{128,130}Xe, ^{102}Pd among others (e.g., [4–7]), have been proposed as possible E(5) candidates, however, in most cases, the experimental evidence was limited. In [7], a list of criteria was proposed, derived from the initial publication by Iachello, to be used as a guideline in search of those nuclei. In particular, the $R_{4/2}$ ratio should be ≈ 2.2, the ratio $B(E2; 4_1^+ \rightarrow 2_1^+)/B(E2; 2_1^+ \rightarrow 0_1^+)$ is expected to be $\approx$1.5 and two excited 0^+ states should exist at approximately 3–4 times the energy of the 2_1^+ state. These 0^+ states should reflect the properties of the 0_ξ^+ and 0_τ^+ states of the E(5) picture [where ξ and τ are quantum numbers that characterize eigenfunctions of the E(5) solution]. In particular, the first excited 0^+ should exhibit an allowed $E2$ transition to the 2_1^+ and a forbidden one to the 2_2^+ state whereas exactly the opposite should stand for the second excited 0^+.

There is an excited 0^+ level at 2052 keV in the level scheme of ^{100}Ru, which decays to the 2_2^+ state with a much stronger $B(E2)$ value than to the 2_1^+ state. This level could be the 0^+ member of the $\tau = 2$ multiplet of the E(5) symmetry. As for the 0_ξ, two possible candidates exist in ^{100}Ru, one at 1130 keV and one at 1741 keV. The first one exhibits a very strong transition to the 2_1^+ as is predicted for the 0_ξ, but it is lower in energy than expected. The second one is closer to the expected energy but its lifetime is so far unknown. Therefore, in order to identify the missing 0_ξ more experimental data are needed.

In the present work, in order to investigate ^{100}Ru as a potential candidate for E(5) symmetry, the fusion-evaporation reaction ^{88}Sr(^{14}C, $2n$)^{100}Ru was used to populate the nucleus.

*Corresponding author: pavel.petkov@nipne.ro

†Present address: Department of Chemistry, Texas A & M University, College Station, Texas, 77843-3144, USA.

‡Present address: Université Frères Mentouri Constantine, 25017 Constantine, Algeria.

§Present address: RIKEN Nishina Center, 2-1 Hirosawa, Wako, Saitama 351-0198, Japan.

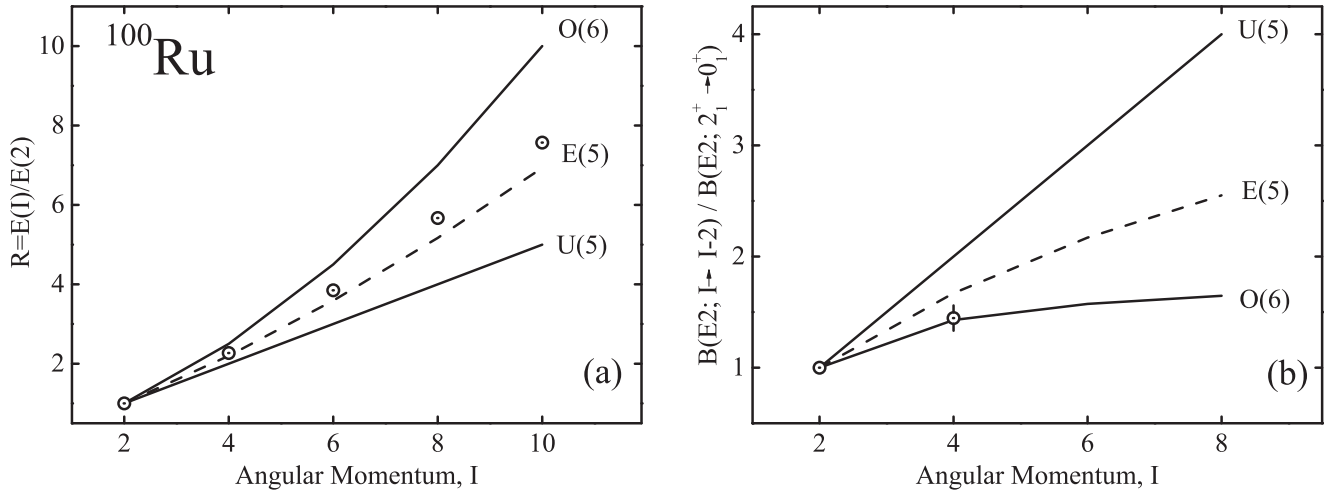

FIG. 1. (a) The energy ratios $E(I_1^+)/E(2_1^+)$ for the yrast band of ^{100}Ru fall almost exactly on the line predicted for the E(5) transitional nuclei. (b) The $B(E2)$ ratios for the transitions of the yrast band of ^{100}Ru. Lack of experimental data does not allow us to draw safe conclusions.

Since, in this case, all the γ-intensity flows early into the yrast band, our experiment cannot address the issue of the 0^+ states but it could extend our knowledge concerning the yrast transitions. In Fig. 1, on the left, one can see the experimental ratios $E(I_1^+)/E(2_1^+)$ of the energies for the yrast levels of ^{100}Ru plotted together with the predictions of the dynamical symmetries U(5) and O(6) (solid lines) and the ones of the E(5) critical point symmetry (dashed line). The experimental energy ratios fall between U(5) and O(6), very close to the predicted values for E(5). The $R_{4/2}$ ratio in particular is 2.27, close to what is expected for an E(5) nucleus. In the same figure, on the right, the known $B(E2)$ ratios are plotted together with the predictions of the aforementioned symmetries. As can be seen, the lack of experimental data above the 4^+ state of the yrast band does not allow for drawing safe conclusions and so the main motivation for this work was to gain more information on the properties of those levels.

In addition with only a few valence protons (four above the $Z = 40$ subshell closure) and neutrons (six above $N = 50$), ^{100}Ru is accessible to shell-model calculations whose reliability was an issue to be checked. New data on transition probabilities could contribute to the systematics of the mass region $A \simeq 100$ and therefore a basis for such calculations describing it in the future.

II. EXPERIMENTAL SET-UP

In order to cover a wide range of lifetimes, the experiment was realized in two parts. First, a recoil distance Doppler shift (RDDS) measurement was performed using the OUPS plunger [8] in order to determine the longer lifetimes (from 1 ps to hundreds of ps) and then a Doppler shift attenuation measurement (DSAM) was performed aiming at the shorter ones in the sub-picosecond region.

As mentioned before, the nucleus of interest was populated in both cases via the fusion-evaporation reaction ^{88}Sr(^{14}C,$2n$)^{100}Ru for which the cross section, according to our calculations with the NRV code [9], peaks at about 200–250 mb at a beam energy of 45 MeV. The $2n$ channel is the second strongest channel after the $3n$ one, which produces ^{99}Ru, whereas the other reaction channels are much weaker. Since none of the energies of the yrast transitions that we are interested overlaps with the ones coming from ^{99}Ru, we considered this reaction as the best possible way to populate the yrast states of ^{100}Ru (for the energies of the yrast levels and transitions of ^{100}Ru see Table I).

Pure Sr is extremely reactive with oxygen, therefore the compound SrF_2 was used instead as the target material. A 0.86 mg/cm^2 thin layer of SrF_2 was evaporated on a Au backing foil. For the RDDS measurement the target was placed with the Au facing the beam and another Au foil was used as a stopper, which was thick enough to stop the ^{100}Ru recoils. For the DSAM measurement the target was flipped over to the other side with the SrF_2 facing the beam so that the Ru recoils would stop in the Au backing whereas the Au stopper foil was removed. The thickness of the Au backing was 1 mg/cm^2 which was thick enough to stop the Ru recoils in the case of the DSAM measurement (where the beam reached the backing after the SrF_2 target) but let the lighter ^{14}C beam particles pass through it with an energy loss of only $\sim$1 MeV for the RDDS measurement (where the beam passed through the backing before reaching the target).

The beam was delivered by the 15 MV Tandem accelerator of the ALTO laboratory in Orsay and the beam intensity was kept $<$1.5 pnA due to dead time limitations of the electronics. For the RDDS measurement a beam energy of

TABLE I. The lifetimes and the corresponding $B(E2)$ values (in W.u. and in e^2fm^4) for the yrast band in ^{100}Ru. The values in bold were determined in the current measurement.

I_i^π	E_x (keV)	τ (ps)	$I_i^\pi \to I_f^\pi$	E_γ (keV)	$B(E2\downarrow)$ (W.u.)	$B(E2\downarrow)$ e^2fm^4
2_1^+	539.510	**31.7(25)**	$2_1^+ \to 0_1^+$	539.509	**20.4(16)**	**561(45)**
4_1^+	1226.465	**3.6(9)**	$4_1^+ \to 2_1^+$	686.972	**54(13)**	**1479(370)**
6_1^+	2075.674		$6_1^+ \to 4_1^+$	849.20		
8_1^+	3060.068	**0.71(15)**	$8_1^+ \to 6_1^+$	984.45	**45(10)**	**42(263)**

46 MeV was chosen so that, after the Au layer, the energy at which the reaction takes place is 45 MeV where the cross section appears to be at its maximum. Data were taken at 12 plunger distances ranging from 1 μm to 1 mm, each run lasting approximately ∼9 h. For the DSAM measurement a beam energy of 40 MeV was chosen so that the ^{100}Ru recoils would stop in the 1 mg/cm^2 Au backing and the irradiation in this case lasted for 18 h.

The detector array was a combination of the ORGAM array housed in Orsay, and eight Miniball detectors of the MINIBALL collaboration that were installed in Orsay for the MINORCA campaign. The ORGAM array was made of 12 HPGe single-crystals, placed at forward angles and arranged in two rings. Four detectors were placed at 72° and eight at 46.5°. The Miniball detectors were mainly installed at backward angles. Each Miniball detector consists of three sixfold segmented HPGe crystals. Eight Miniball detectors in total were mounted at angles ranging from about 90° up to 161°. The total efficiency for the whole array was measured 7.3% at 1.3 MeV, most of which is due to the Miniball detectors.

The data were recorded by use of digital electronics, which consisted of 56 digital gamma finder (DGF) cards with four channels each. Within those cards, each signal is firstly amplified with software-controlled gain and offset, digitized by a sampling ADC and then all processing operations including filtering, triggering and pulse shape analysis are performed in a numerical way [10]. A total amount of about 6.5 × 10^8 γ-γ coincidences were recorded for the DSAM measurement and about half of that for each distance of the RDDS measurement.

III. DATA ANALYSIS AND RESULTS

For the subsequent analysis, the data were arranged in several ring-wise γ-γ matrices using ROOT [11]. The definition of those matrices is straightforward for the case of the ORGAM detectors which were already arranged at known polar angles but not for the Miniball detectors. Firstly, they were not arranged in rings but each one was placed individually in order to obtain the best possible angular coverage at backward angles. Secondly, because of their size, they cover a very big angular range and cannot be considered as lying at an unique polar angle. It was thus decided to treat each segment of each Miniball detector as a separate detector with its own polar angle. The segments were then grouped into rings with angular ranges of 10° for the analysis. The ring with the most segments and thus the most statistics was the one at 145° ± 5 which is a reasonably large backward angle to observe the Doppler shift of the γ rays and therefore it was chosen as the preferred ring for the backward angle projections.

A. Doppler shift attenuation method and data analysis

The Doppler shift attenuation method (DSAM) is based on the Doppler shift of the γ rays emitted while the recoil decelerates in the target, as observed by the detectors placed in forward or backward angles. The lineshape of the photopeak of the γ ray of interest is affected by the stopping power of the material, the initial velocity of the recoil, the feeding of the level and of course the lifetime in question. The range of lifetimes that can be measured by this technique depends on the stopping time of the recoils in the material of the target stopper. In our case, the initial velocity of the ^{100}Ru recoils is calculated to be 0.9% of the velocity of light. For this value of the ratio v/c and for the target described in the previous section the calculated distribution of the stopping times of the recoils in the target is shown in Fig. 2. As can be seen, our experimental set-up is well calibrated to measure lifetimes of the order of 1 ps or lower.

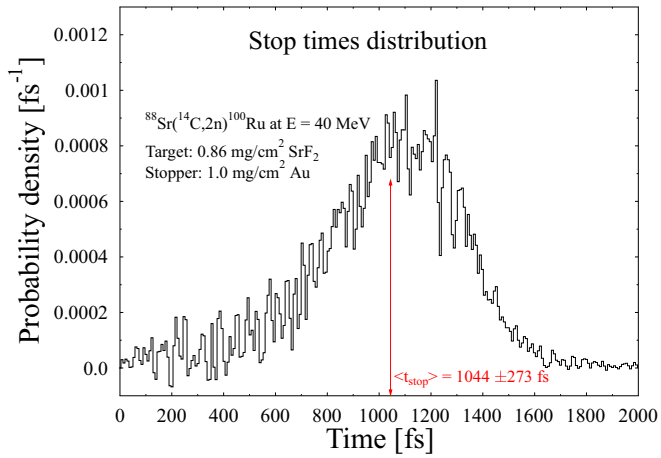

FIG. 2. The distribution of the stopping times of the ^{100}Ru recoils in the target-stopper material. As can be seen, lifetimes of the order of 1 ps or lower can be measured with this technique.

The lineshapes were simulated using the DSAM code employed, e.g., in [12,13] which uses the description of the slowing down process presented in [14,15] on the basis of modifications of the Monte Carlo code DESASTOP written by Winter [16,17]. The simulation takes into account nuclear and electron stopping powers of the target and the stopper including the elemental consistency of the target, the cross section of the reaction, the reaction kinematics, the detector resolution (FWHM), the finite size of the detector (solid angle) and the neutron emission spectra. Further, for the lineshape analysis, the natural time-dependent functional form of the population $n_i(t)$ of the investigated level as a solution of the Bateman equations was used, namely,

$$n_i(t) = \sum_{k \geqslant i} C_{ik} \exp(-\lambda_k t), \qquad (1)$$

which represents a superposition of exponentials with coefficients C_{ik} determined by the decay constants λ_k, by the branching ratios and by the initial population of the kth level participating in the cascade.

In the most general case, a fitting procedure, which aims at determining multiple decay constants simultaneously, is confronted with the difficulty to find a multiparameter solution, including some parameters describing the nonobserved or side-feeding. For the present case of the $I^\pi = 8^+$ level it was established that there are mainly two feeding paths that have to be included, one of them being "slow" and the other "fast".

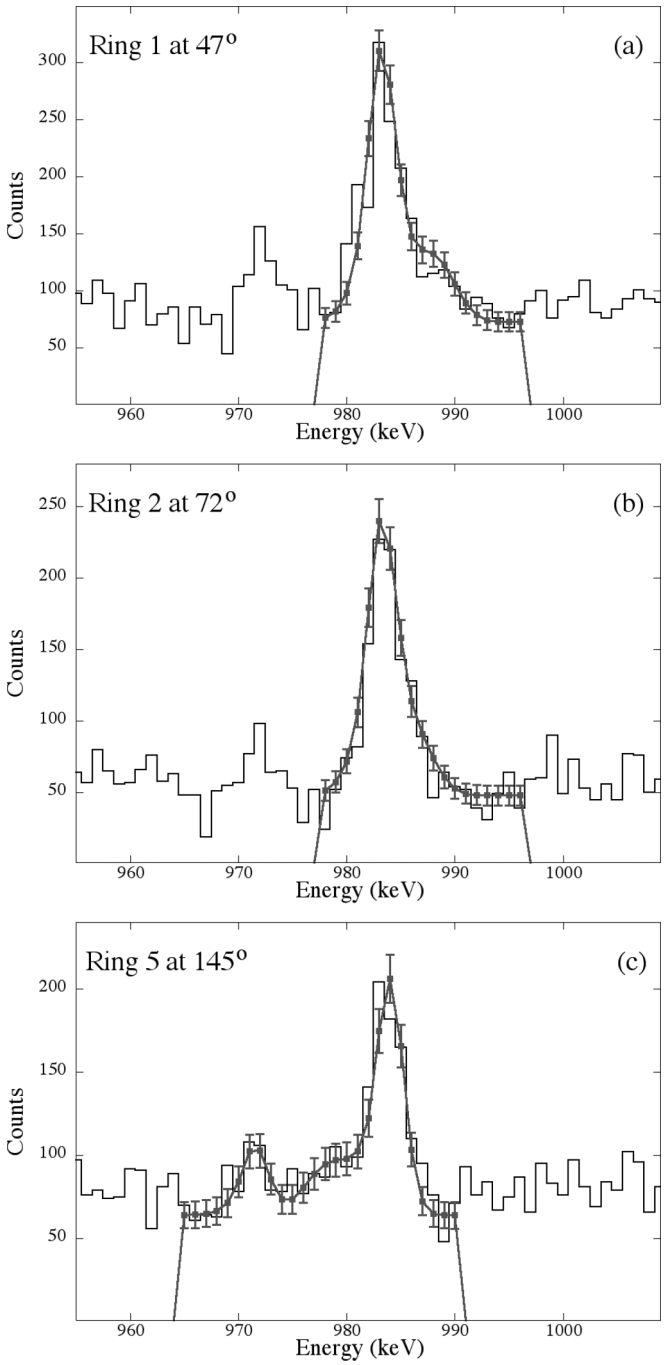

FIG. 3. The DSAM fit of the lineshape of the 984 keV peak for the three angles at (a) 46.5°, (b) 72°, and (c) 145° is shown.

Thus, the only remaining parameter to be determined is the decay constant of the level of interest.

In total, three angles were used for the analysis, the two forward angles at 46.5° and 72° and the backward angle at 145°. The lineshape for the $8_1^+ \rightarrow 6_1^+$ transition at 984 keV was simulated for these three angles and was fitted to match the experimental spectra. The comparison can be seen in Fig. 3. A χ^2-minimization procedure was followed to estimate the best fit as well as the error. Keeping the rest of the parameters fixed, the lifetime was incrementally changed with a step of 5 fs and

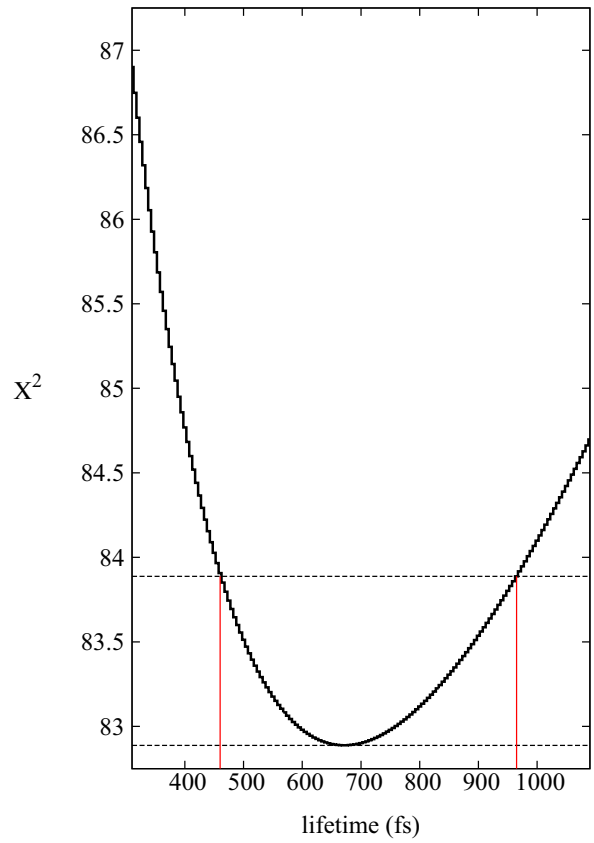

FIG. 4. The χ^2-minimization procedure which was used to determine the lifetime and its error. Having fixed the rest of the parameters of the simulation, the lifetime is left as a free parameter and it is then plotted against the non-reduced χ^2 value on the vertical axis. The minimum gives the lifetime value of the level whereas the error is given by the range of lifetimes obtained by incrementing the χ^2 value by one unit.

the χ^2 value of the fit was recorded. In Fig. 4 one can see the χ^2 value of the fit as a function of the lifetime for the case of the ring at 72°. Incrementing the χ^2 value by one unit provides the often used estimate of the error of the measurement (see, e.g., [18]). This is shown clearly in Fig. 4. Similar plots were obtained for the other two angles and the weighted average of the three lifetime values obtained was

$$\tau_{8^+} = 710 \pm 150 \text{ fs}$$

For the lower-lying yrast states no lineshape was observed which means that their lifetimes lie above the 1 ps sensitivity of this technique. For these lifetimes the RDDS method described in the next paragraph is more suitable.

B. Recoil distance Doppler shift method and data analysis

The RDDS method is a well known technique applied for the determination of lifetimes of excited nuclear states in the region above 1 ps (for a detailed presentation see, e.g., Ref. [19] and references therein). It basically uses the timing information involved in the splitting of the intensity of a depopulating γ-ray transition into components characterized by different Doppler

shifts. The γ rays emitted in flight by the nuclei recoiling from the target are detected with a Doppler-shifted energy and give rise to the shifted (S) component in the spectrum. Emissions occurring with the nucleus at rest in the stopper contribute to the unshifted (U) component. The evolution of the intensity splitting of the two components as a function of the target-to-stopper distance is sensitive to the lifetime τ of the depopulated level. Therefore the determination of the areas of the U and S peaks is of primordial importance for the analysis of RDDS data. Its precision in practical cases was considered in detail in Ref. [15]. Here we only mention few points which are relevant for the present measurement. Some difficulties arise when the two peaks are not well separated due to a small Doppler shift as in our case. Then, their lineshapes have to be known in order to disentangle the U and S contributions. The shape of the U peak is described only by the response function of the detector, but the shape of the S peak depends also on the velocity distribution of the recoiling nuclei which is determined by the target thickness and stopping powers, the reaction kinematics, and the beam energy. In our specific experiment, due to relatively small recoil velocity and large target thickness, part of the recoils, which is estimated by our simulation to be 6–8%, was stopped in the target. This effect which is more visible in the fit of the 2_1^+ state was taken into account in the analysis. Additionally, the shape of the S peak is to some extent distance-dependent since the faster recoils reach the stopper in a shorter time than the slower ones and therefore contribute less to the S peak, especially at short distances. Finally, the recoiling nuclei need a finite time interval (typically about 1 ps) to come to rest in the stopper and during the slowing-down, the Doppler-shift of the emitted γ rays is attenuated which gives rise to a continuous (DSA) spectrum.

In Ref. [15], a procedure was proposed to solve these problems for the case of coincidence RDDS measurements where a gate is set on the shifted component of a transition directly feeding the level of interest. In the present work however, it was not possible to use such a gate without a significant loss of statistics. Therefore we used a variant of the procedure described in Ref. [20] which is relevant in the case where the gating condition does not influence the timing information for the investigated level. Namely, in order to deduce the intensities of the transition of interest and of a feeding transition, gates were set on the complete line (both shifted and unshifted components included) of the feeding transition and of the transition of interest, respectively. In this way, the problem with the unknown (unobserved) feeding was solved by using coincidences of a feeding transition with the transition of interest. To increase statistics, we summed up the spectra corresponding to gates set in the three independent rings. The influence of possible deorientation effects (see, e.g., Ref. [21]), on the analysis was estimated to be negligible due to the relatively small lifetimes determined.

As discussed in Ref. [20], after the creation of the excited nucleus at time $t = 0$, the transition of interest can occur in four physically distinct cases: during the motion in the target finishing at t_{f_i}, during the flight in vacuum which ends at t_{f_f}, during the slowing-down in the stopper completed at t_s and after coming to rest. Correspondingly, four different components contribute to the spectrum.

To apply the formalism of Ref. [20] in practice, we performed a three-dimensional Monte Carlo (MC) simulation of the time evolution of the recoil velocity distribution by describing the processes of the creation of the recoils, the slowing-down in the target, the free flight in vacuum and the slowing-down in the stopper. Further, the "velocity histories" were randomized with respect to the registering detectors. The modified version of the computer code DESASTOP quoted in the previous section was used for the Monte Carlo simulation. At large distances, the lineshapes of the shifted peaks were satisfactorily reproduced and therefore one can conclude that the stopping powers of the target material were correctly taken into account. It is reminded that only at large distances these lineshapes are fully representative of the underlying velocity distribution of the recoiling nuclei. A summation over several thousands MC histories is sufficient for a correct reproduction of the lineshapes. In the procedure for the analysis, the background-subtracted lineshapes corresponding to the transition of interest at all distances and the shifted decay curve

$$S_{af}(t) = b_{af} \int_0^t \lambda_a n_a(t')dt' \tag{2}$$

are fitted simultaneously.

The "unshifted" decay curve is given by the complementary integral:

$$R_{af}(t) = b_{af} \int_t^\infty \lambda_a n_a(t')dt' = S_{af}(\infty) - S_{af}(t). \tag{3}$$

In Eqs. (2) and (3), $n_a(t)$ is the time-dependent population of the level of interest a, λ_a is its decay constant (the lifetime $\tau_a = 1/\lambda_a$) and b_{af} is the branching ratio of the transition $a \rightarrow f$. In the analysis, the function $S_{af}(t)$ is represented by continuously interconnected second-order polynomials over an arbitrarily chosen set of neighboring time intervals. The fitting problem is linear with respect to the polynomial parameters and the areas of the unshifted peak. The fitting procedure is performed by changing the limits of the time-intervals until the best reproduction of the experimental spectra is achieved.

For singles RDDS measurements, the differential decay curve method (DDCM) [22] provides an expression for the lifetime of the level of interest τ_a at every distance x or flight time $t = x/v_z$:

$$\tau_a(t) = \left(R_{af}(t) - b_{af} \sum_{h=1}^{N} (1 + \alpha_{ha}) R_{ha}(t) \right) \Big/ (b_{af} \lambda_a n_a(t)). \tag{4}$$

The numerator yields the number of nuclei $n_a(t)$ at time t which decay via the transition $a \rightarrow f$ (cf. Ref. [22]). The quantities α_{ha} are the internal conversion coefficients of the γ-ray transitions $h \rightarrow a$ and the sum runs only over the direct feeders h of the level a. The denominator represents the first derivative of the shifted decay curve $S_{af}(t)$ or the decay function of the transition $a \rightarrow f$. It should be mentioned that Eq. (4) can be used also in coincidence, when the gate does not influence the lifetime information as in the case of the present analysis. In Ref. [20], it is shown that taking into account the velocity distribution and DSA effects leads to an

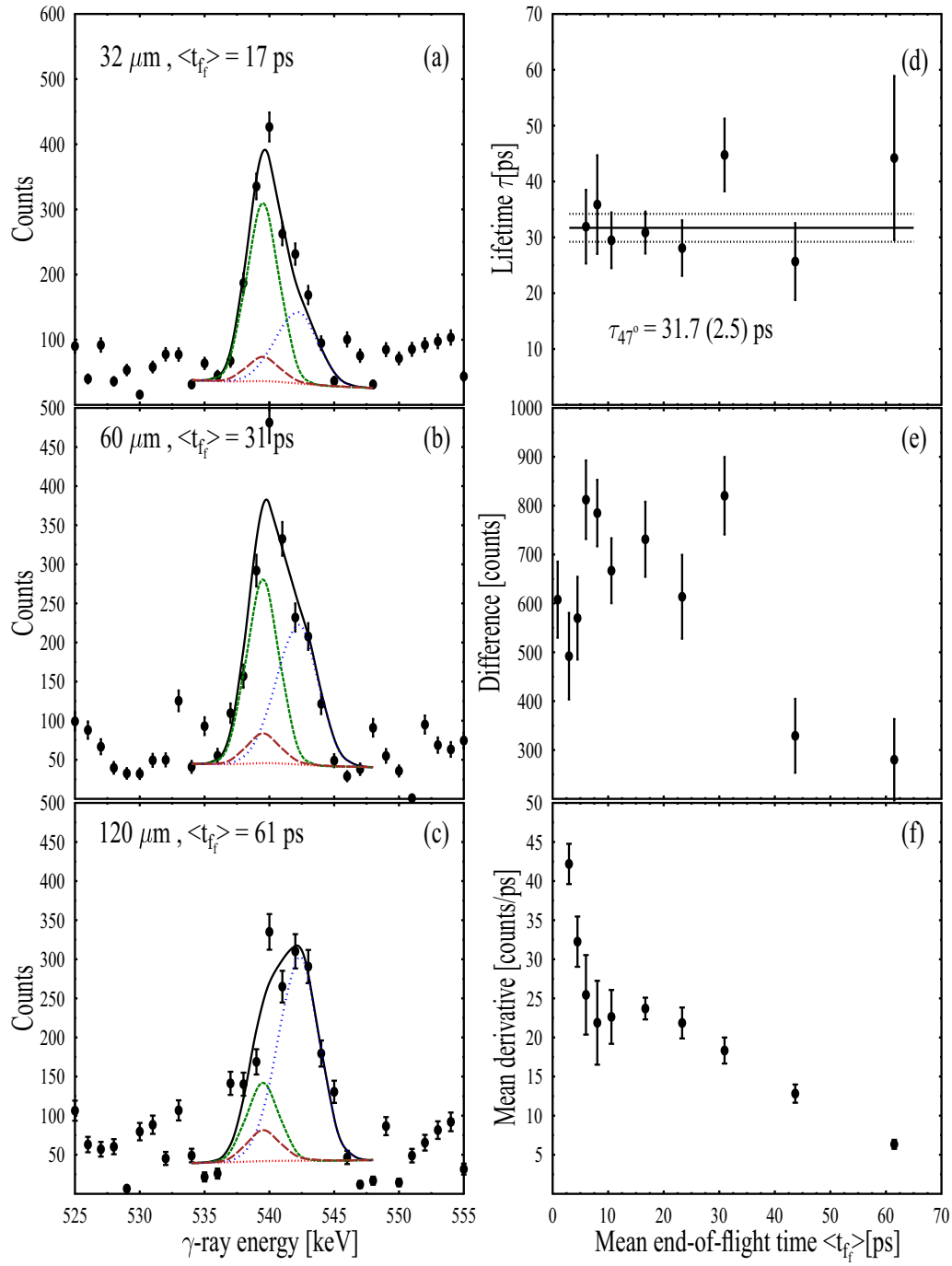

FIG. 5. Example of the lifetime analysis of the 540 keV transition gated on the 687 keV transition as observed at 46.5°. The fits in the left panels [(a)–(c)] illustrate the contributions of the shifted peak (blue dotted line), unshifted peak (green short-dashed line), and decays in the target and DSA-effects (red dot-dashed line). In (d), the τ curve is displayed. It is a result of the division of the numerator in Eq. (5) (e) by the corresponding denominator (f). See text for details.

equation for each distance x or mean end-of-flight time $\langle t_{f_f} \rangle$ which reads

$$\tau(x) = \tau(\langle t_{f_f} \rangle) = \left(\tilde{R}_{af}(x) - b_{af} \sum_{h=1}^{N} (1 + \alpha_{ha}) \frac{I^{\gamma}_{ha} \tilde{S}_{af}(\infty)}{I^{\gamma}_{af} \tilde{S}_{ha}(\infty)} \tilde{R}_{ha}(x) \right) \Big/ \times \langle d\tilde{S}_{af}/dt|_{t=t_s} \rangle. \quad (5)$$

Here, the quantities I^{γ} are the relative intensities of the γ-ray transitions and $\tilde{S}(\infty)$ are the values of the fitted shifted decay curves at large times (i.e., when they reach constant values). The γ-ray intensities have to be known independently.

In Eq. (5), the quantities $\tilde{R}$ are the areas of the corresponding unshifted peaks whereas the denominator represents the derivative $d\tilde{S}_{af}(t)/dt$ averaged over the MC histories used for the fits of the RDDS spectra and $\tilde{S}_{af}(t)$. The final result

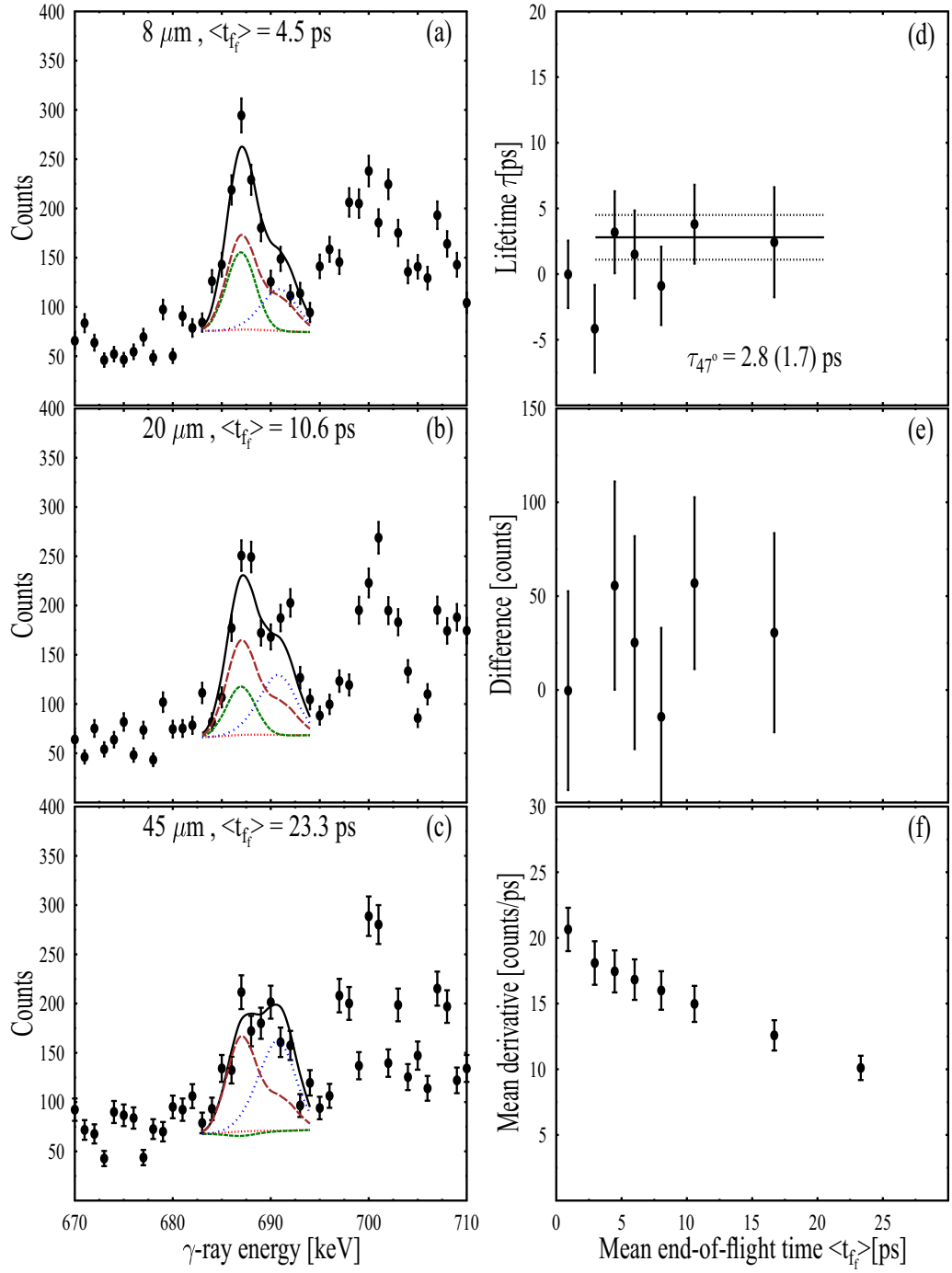

FIG. 6. Example of the lifetime analysis of the 687 keV transition gated on the 849 keV transition as observed at 46.5°. As in the 2^+-tauplot, the fits in the left panels [(a)–(c)] illustrate the contributions of the shifted peak (blue dotted line), unshifted peak (green short-dashed line), and decays in the target and DSA-effects (red dot-dashed line). The τ curve is displayed in (d). It is a result of the division of the numerator in Eq. (5) (e) by the corresponding denominator (f).

for the lifetime, in the spirit of [22], is obtained by fitting a straight line through the points calculated following Eq. (5) (the τ curve) within the region of sensitivity where the values are reliable. Deviations of the τ curve from a straight line in this region point to systematic errors in the analysis and give a feedback information for improvements.

In order to deduce the intensities of the transition of interest and of the feeding yrast transition to the 2^+ level, spectra gated on the complete line (both shifted and unshifted components included) of these transitions were analysed. Due to problems with contaminations, only the coincident pairs Ring 1 against Ring 1 were used in the analysis as illustrated in Fig. 5. The resulting value for the lifetime of the 2_1^+ is

$$\tau(2_1^+) = 31.7(25)\ \text{ps}.$$

TABLE II. $B(E2)$ systematics for the nuclei with $N = 56$ and Z varying from the subshell closure of $Z = 40$ to the shell closure of $Z = 50$ as taken from the existing literature. The transition strengths deduced in this work for ^{100}Ru are shown with bold letters. All the $B(E2)$ values are given in W.u.

$I_i^\pi \rightarrow I_f^\pi$	$^{94}_{38}$Sr [28]	$^{96}_{40}$Zr [29]	$^{98}_{42}$Mo [30]	$^{100}_{44}$Ru	$^{102}_{46}$Pd [31]	$^{104}_{48}$Cd [32]	$^{106}_{50}$Sn [33]	$^{108}_{52}$Te [34]
$2_1^+ \rightarrow 0_1^+$	8 (3)	2.3 (3)	19.8 (4)	**20.4 (16)**	30.4 (7)	26.7 (10)	13.2 (26)	25 (3)
$4_1^+ \rightarrow 2_1^+$	>1.4		42.2 (9)	**54 (13)**	40.3(29)	47 (16)		
$6_1^+ \rightarrow 4_1^+$			10.1 (4)[a]		35.5 (17)			
$8_1^+ \rightarrow 6_1^+$				**45 (10)**	24.9 (29)			

[a]Uncertainty about the spin assignment.

This value disagrees with the adopted value of 18.1(2) ps [23] but it is in agreement with an older measurement of Temmer *et al.* [24] where a value of 30 ps is reported. It is also in good agreement with our theoretical calculations shown in the following section. In addition, it is worth noting that all previous measurements of the 2_1^+ of ^{100}Ru (namely [24–27]) were Coulomb excitation experiments where the absolute measurement of the beam current is a very challenging issue. Also, the involvement of the reorientation effect in such measurements is especially pronounced at the 2_1^+ and can lead to errors. Moreover, to determine lifetimes in the range of ps the plunger method is expected to be much more accurate. For those reasons we consider our value as more precise and reliable.

In the case of the $I^\pi = 4^+$ level, the statistics were sufficient to employ gates on both full lineshapes of the 849 keV and 687 keV γ-ray transitions and therefore the side-feeding did not influence the analysis. The results obtained at the different rings were averaged to yield the result

$$\tau(4_1^+) = 3.6(9).$$

We note that the presently derived lifetime of the 4^+ level is in perfect agreement with the result from the literature $\tau = 3.75(29)$ ps. To illustrate the analyzing procedure, we show in Fig. 6 an example of the analysis of the data for the 687 keV transition, which depopulates the $I^\pi = 4^+$ level of the yrast band. In the left panels of the figures, lineshapes measured at the indicated distances are displayed together with the fits at the corresponding angle. We note that the decays in the target and DSA effects are also taken into account. The lifetime derivation is shown in the right panels. The final result for the lifetime is obtained by averaging the values derived at the different rings, always paying attention to possible systematic errors (see, e.g., Ref. [20]).

In the case of the $I^\pi = 6^+$ state the statistics did not allow us to safely determine a lifetime through RDDS whereas its lifetime does not appear to be short enough for a lineshape DSAM analysis as in the case of the $I^\pi = 8^+$. In addition, at backward angles the RDDS analysis is hindered by a gamma-line at 847 keV coming from ^{56}Fe excited in the laboratory environment during the experiment. We can safely say however, based on the stopping time of the ^{100}Ru recoils shown in Fig. 2, that its lifetime is >1 ps.

To check for possible deorientation effects (see, e.g., Ref. [21]), we considered the behavior of the sum of the shifted and unshifted components as function of the target-to-stopper distance. No deviation from a constant behavior was found within the error bars. Therefore we conclude that the present results are not affected by the deorientation and give a conservative estimate of 5% from the values of the derived lifetimes.

The lifetimes deduced in this work for ^{100}Ru as well as the corresponding $B(E2)$ values are shown in Table I. Also, in Table II, the deduced transitions strengths for ^{100}Ru are compiled together with those of the neighboring $N = 56$ isotones.

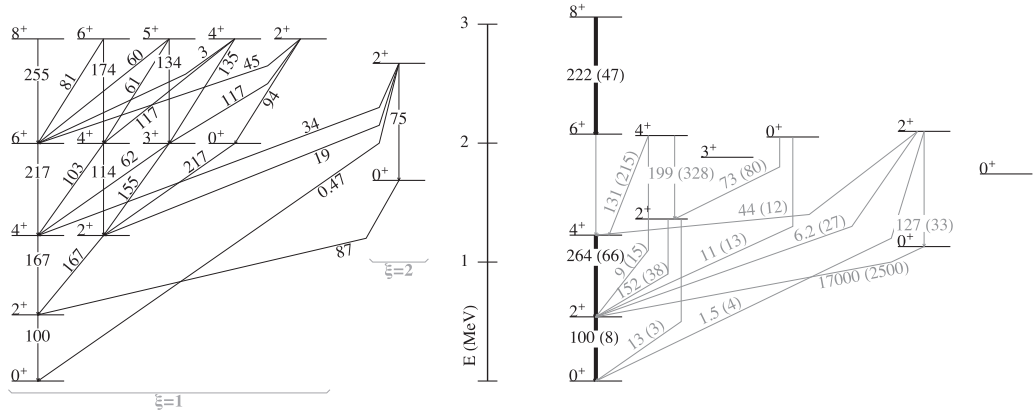

(a) E(5) (b) ^{100}Ru

FIG. 7. The level scheme of ^{100}Ru plotted next to the E(5) level scheme. The transition strengths are normalized to the value $B(E2; 2_1^+ \rightarrow 0_1^+)$ which is set to 100 arb. units in order to facilitate the comparison of the two.

IV. DISCUSSION

The results of our analysis are compared to the E(5) predictions in Fig. 7. The values measured for the yrast band do not seem to be in good agreement with them. In particular the ratio $B(E2;4_1^+ \rightarrow 2_1^+)/B(E2;2_1^+ \rightarrow 0_1^+)$ is 2.64 according to our measurement to be compared with the value 1.67 predicted by the E(5) critical point symmetry. The discrepancy is not as bad for the decay of the 8^+ but the increasing trend of the $B(E2)$s in the yrast band predicted by the E(5) is not verified in our measurement.

It should be mentioned here that there are other solutions of the Bohr-Hamiltonian that seem to agree better with our measured ratios. In particular, a recent review on solutions of the Bohr Hamiltonian with the sextic potential, appropriate for a variety of nuclei, can be found in [35]. The $^{98-108}$Ru isotopes, in particular, have been considered in the framework of the X(3)-sextic solution [36]. The prediction given there for the ratio $B(E2;4_1^+ \rightarrow 2_1^+)/B(E2;2_1^+ \rightarrow 0_1^+)$ is 2.23 which is the closest one to the 2.64 value found in the present work. Also, a detailed study of $B(E2)$ transition rates of the $^{98-104}$Ru isotopes in the framework of the Bohr Hamiltonian with the Manning-Rosen potential is given in [37]. In Table 3 of [37] the predictions of the Bohr Hamiltonian with several other potentials (Morse, Davidson, Kratzer) are given. It is worth noticing that the Manning-Rosen potential provides for the ratio $B(E2;8_1^+ \rightarrow 6_1^+)/B(E2;2_1^+ \rightarrow 0_1^+)$ the value of 2.28, which is very close to the value of 2.21 found in the present manuscript. However, these are isolated points of success. As a rule, in the Bohr collective model, $B(E2)$s along the ground state band get increasing without exception and that disagrees with our observations for ^{100}Ru. This disagreement could be due to the fact that $^{100}_{44}$Ru is close to a subshell closure for protons and close to a shell closure for neutrons and therefore may be better described within the framework of other models which take into account specific structural effects not included in E(5) or in other solutions of the Bohr-Hamiltonian. This conclusion is also supported by the fact that a similar trend of the $B(E2)$s is observed in the neighboring nuclei as can be seen in Table II.

Therefore, although our initial goal was to test this nucleus as an E(5) candidate, we were prompted to further inspect the structure of ^{100}Ru using two different approaches. In the first approach the nucleus was studied with the excited Vampir variational model and the second approach was a standard nuclear shell-model calculation with the code NUSHELLX@MSU. These two calculations are presented in the following paragraphs.

A. Excited Vampir calculations

The structure of neutron-rich nuclei in the $A \simeq 100$ mass region manifests drastic changes in some isotopic chains and often sudden variations of particular nuclear properties have been identified. Neutron-rich Sr and Zr nuclei indicate rapid transition from spherical to deformed shape with a possible identification of triple shape coexistence in the $N = 58$ ^{96}Sr and ^{98}Zr [38]. The evolution in structure with increasing spin in ^{100}Ru was studied within the *complex* excited Vampir

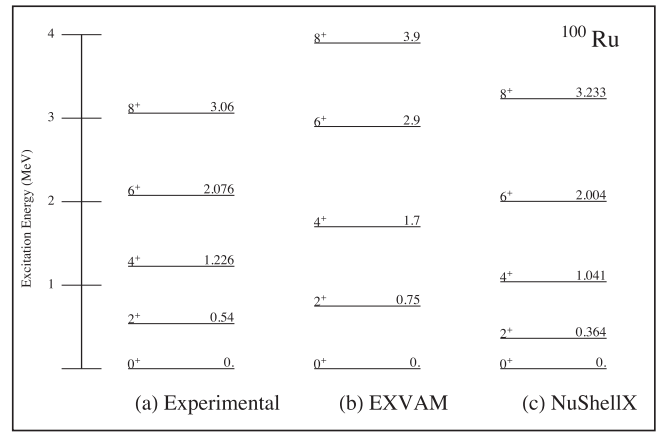

FIG. 8. The comparison of the experimental level scheme of the yrast band (a), to the ones calculated with EXVAM (b) and NUSHELLX (c).

(EXVAM) variational model with symmetry projection before variation using a realistic effective interaction based on Bonn CD potential in a large model space [38].

For nuclei in the $A \simeq 100$ mass region a rather large model space is used above the ^{40}Ca core built out of $1p_{1/2}$, $1p_{3/2}$, $0f_{5/2}$, $0f_{7/2}$, $2s_{1/2}$, $1d_{3/2}$, $1d_{5/2}$, $0g_{7/2}$, $0g_{9/2}$, and $0h_{11/2}$ oscillator orbits for both protons and neutrons in the valence space. The effective two-body interaction is constructed from a nuclear matter G matrix based on the Bonn CD potential. In order to enhance the pairing properties, the G matrix was modified by three short-range (0.707 fm) Gaussians for the isospin $T = 1$ proton-proton, neutron-neutron, and neutron-proton matrix elements with strengths of -40, -30, and -35 MeV, respectively. The isoscalar spin 0 and 1 particle-particle matrix elements are enhanced by an additional Gaussian with the same range and the strength of -70 MeV. In addition the isoscalar interaction was modified by monopole shifts for all $T = 0$ matrix elements of the form $\langle 0g_{9/2}0f;IT = 0|\hat{G}|0g_{9/2}0f;IT = 0\rangle$ involving protons and neutrons occupying the $0f_{5/2}$ and the $0f_{7/2}$ orbitals. The Coulomb interaction between the valence protons was added.

The lowest positive parity states up to spin 8^+ in ^{100}Ru were calculated including in the excited Vampir many-nucleon bases up to 14 EXVAM configurations. The final solutions for each spin have been obtained diagonalizing the residual interaction between the considered excited Vampir configurations.

The theoretical lowest band of ^{100}Ru is compared to the experimental spectrum in Fig. 8(b). The $E2$ transition strengths (calculated using the effective charges $e_p = 1.3$ and $e_n = 0.3$ [38]) are compared to the ones measured in the current work in Fig. 9.

B. Shell-model calculations

Shell-model calculations were also performed with the NUSHELLX@MSU [39] code, using the $jj45pna$ interaction which is composed of four parts (proton-proton, neutron-neutron, and proton-neutron interactions as well as a Coulomb repulsive term). The $jj45pn$ valence space used includes four proton orbits ($f_{5/2}$, $p_{3/2}$, $p_{1/2}$, $g_{9/2}$) and five neutron orbits

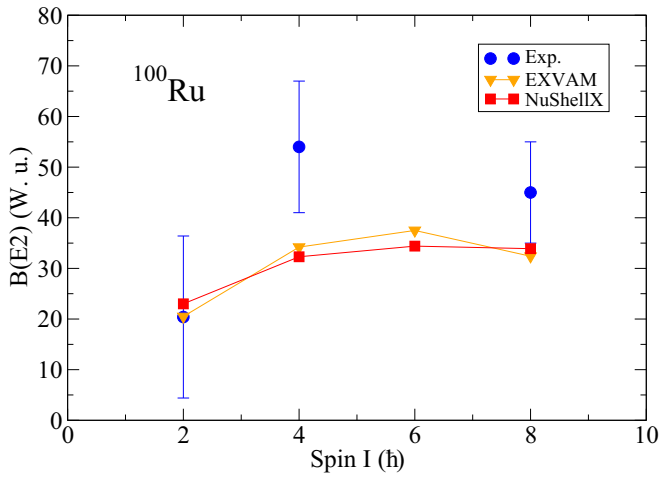

FIG. 9. The comparison of the experimental transition strengths of the yrast band measured in this work (circles), to the ones calculated with EXVAM (triangles) and NUSHELLX (squares).

$(g_{7/2}, d_{5/2}, d_{3/2}, s_{1/2}, h_{11/2})$, suitable for the description of nuclei with $28 \leqslant Z \leqslant 50$ and $50 \leqslant N \leqslant 82$. The calculations have been made up to $I = 8$.

As the calculations of $^{100}_{44}$Ru lead to too large dimensions to be performed in the full $jj45pn$ space, we made a truncation of the neutron valence space by always keeping the $\nu h_{11/2}$ orbit empty. We presume that this constitutes a pertinent truncation for the description of the lowest excited states of ^{100}Ru, since the $\nu h_{11/2}$ orbit is expected to be involved only for states having higher spins and located at high excitation energies.

As can be seen in Fig. 8(c), the calculations underestimate the experimental values of the 2_1^+ and 4_1^+ excitation energies by about 180 keV. The agreement is better for the 6_1^+ state. On the other hand, the 8_1^+ state is calculated 173 keV above its experimental counterpart. A more detailed analysis of the wave functions of the calculated levels shows that these four states present similar characteristics. In average they are very mixed. Five of the six valence neutrons always occupy the $\nu g_{7/2}$ and $\nu d_{5/2}$ first two orbits, whereas the $\nu d_{3/2}$ and $\nu s_{1/2}$ "share" the sixth one. It is worth noting that this justifies *a posteriori* the truncation performed in the calculations. As for the 16 valence protons, the occupation of the orbits is also almost identical for the yrast sequence. The proton configuration can thus be expressed as $(f_{5/2})^5(p_{3/2})^3(p_{1/2})^1(g_{9/2})^7$. For each spin, it is interesting to notice that both neutron and proton orbits contribute to establish the final angular momentum. Whereas the main contribution, about 60%, comes from the neutrons, a proton pair is also broken in most of the configurations and brings up to 4 units of angular momentum. As well, the decomposition of the 0^+ ground state wave function shows that the main part (52%) comes from couplings of $J = 2$ protons and neutrons. $(J_\pi = 0,\ J_\nu = 0)$ couplings only account for 28% of the wave function, and $(J_\pi = 4,\ J_\nu = 4)$ couplings are also involved (16%).

In addition, $B(E2\downarrow)$ transition probabilities have been calculated for the 2^+, 4^+, 6^+, and 8^+ yrast states, using the effective charges $e_p = 1.5$, $e_n = 0.5$. The obtained values, shown in Fig. 9(c), express both the large configuration mixings and the resemblance of the calculated states. $B(E2\downarrow)$ values are indeed calculated almost identical for the 4_1^+, 6_1^+, and 8_1^+ state.

In Fig. 8 one can see that the NUSHELLX calculation is closer to the experimental excitation energies than the EXVAM one where the energies appear to be more stretched. However, in Fig. 9 where the measured $B(E2)$ values are compared to the calculated ones within the two models, we can see that they are in good agreement to each other and, most importantly, the experimental trend is reproduced by both calculations, with an increase between spins 2^+ and 4^+, and a slight decrease at spin 8^+.

C. Conclusions

The nucleus ^{100}Ru was studied by measuring the lifetimes of the 2_1^+, 4_1^+, and 8_1^+ levels of the yrast band. It is shown that this nucleus may not be the best candidate for E(5) critical point symmetry, on the basis of the experimental $B(E2)$ ratios. Further investigations of the structure of the nucleus were carried out by means of two theoretical approaches, excited Vampir and shell model. There is a good agreement between the two calculations and the trend manifested in the experimental data.

ACKNOWLEDGMENTS

This work was partially supported by a grant of the Romanian National Authority for Scientific Research, CNCS-UEFISCDI, Project No. PN-II-ID-PCE-2011-3-0153 and the Bulgarian National Science Fund under Contract No. DFNI-E02/6. This work was also partly supported by the German BMBF under Contracts No. 05P12PKFNE and No. 05P15PKCIA. A.G. was supported by the P2IO Excellence Laboratory.

[1] F. Iachello, Phys. Rev. Lett. **85**, 3580 (2000).
[2] F. Iachello, Phys. Rev. Lett. **87**, 052502 (2001).
[3] R. F. Casten and N. V. Zamfir, Phys. Rev. Lett. **85**, 3584 (2000).
[4] A. Frank, C. E. Alonso, and J. M. Arias, Phys. Rev. C **65**, 014301 (2001).
[5] D. Zhang and Y. Liu, Chin. Phys. Lett. **20**, 1028 (2003).
[6] N. V. Zamfir, M. A. Caprio, R. F. Casten, C. J. Barton, C. W. Beausang, Z. Berant, D. S. Brenner, W. T. Chou, J. R. Cooper, A. A. Hecht, R. Krücken, H. Newman, J. R. Novak, N. Pietralla, A. Wolf, and K. E. Zyromski, Phys. Rev. C **65**, 044325 (2002).
[7] R. M. Clark, M. Cromaz, M. A. Deleplanque, M. Descovich, R. M. Diamond, P. Fallon, I. Y. Lee, A. O. Macchiavelli, H. Mahmud, E. Rodriguez-Vieitez, F. S. Stephens, and D. Ward, Phys. Rev. C **69**, 064322 (2004).
[8] J. Ljungvall, G. Georgiev, S. Cabaret, N. Karkour, D. Linget, G. Sedes, R. Chevrier, I. Matea, M. Niikura, M.-D. Salsac, and B. Sulignano, Nucl. Instrum. Methods Phys. Res. A **679**, 61 (2012).
[9] V. I. Zagrebaev, A. S. Denikin, A. V. Karpov, A. P. Alekseev, M. A. Naumenko, V. A. Rachkov, V. V. Samarin, and V. V.

Saiko, NRV web knowledge base on low-energy nuclear physics, http://nrv.jinr.ru/.
[10] J. Eberth, G. Pascovici, H. G. Thomas, N. Warr, D. Weisshaar, D. Habs, P. Reiter, P. Thirolf, D. Schwalm, C. Gund, H. Scheit, M. Lauer, P. Van Duppen, S. Franchoo, M. Huyse, R. M. Lieder, W. Gast, J. Gerl, K. P. Lieb, and the MINIBALL Collaboration, *Frontiers of Nuclear Structure* (American Institute of Physics, New York, 2003), Vol. 656, p. 349.
[11] R. Brun and F. Rademakers, *Proceedings of the AIHENP'96 Workshop, Lausanne* [Nucl. Instrum. Methods Phys. Res. A **389**, 81 (1997)].
[12] J. N. Orce, P. Petkov, C. J. McKay, S. N. Choudry, S. R. Lesher, M. Mynk, D. Bandyopadhyay, S. W. Yates, and M. T. McEllistrem, Phys. Rev. C **70**, 014314 (2004).
[13] A. Astier, P. Petkov, M.-G. Porquet, D. S. Delion, and P. Schuck, Phys. Rev. Lett. **104**, 042701 (2010).
[14] P. Petkov, J. Gableske, O. Vogel, A. Dewald, P. von Brentano, R. Krücken, R. Peusquens, N. Nicolay, A. Gizon, J. Gizon, D. Bazzacco, C. Rossi-Alvarez, S. Lunardi, P. Pavan, D. R. Napoli, W. Andrejtscheff, and R. V. Jolos, Nucl. Phys. A **640**, 293 (1998).
[15] P. Petkov, D. Tonev, J. Gableske, A. Dewald, T. Klemme, and P. von Brentano, Nucl. Instrum. Methods Phys. Res. A **431**, 208 (1999).
[16] G. Winter, ZfK Rossendorf Report No. ZfK-497 (1983).
[17] G. Winter, Nucl. Instrum. Methods **214**, 537 (1983).
[18] Robley D. Evans, *The Atomic Nucleus* (McGraw-Hill, New York, 1969), Chap. 27.
[19] T. K. Alexander and J. S. Forster, Adv. Nucl. Phys. **10**, 197 (1978).
[20] P. Petkov, A. Dewald, R. Kühn, R. Peusquens, D. Tonev, S. Kasemann, K. O. Zell, P. von Brentano, D. Bazzacco, C. Rossi-Alvarez, G. de Angelis, S. Lunardi, P. Pavan, and D. R. Napoli, Nucl. Phys. A **674**, 357 (2000).
[21] G. Goldring, in *Heavy Ion Collisions*, edited by R. Bock (North-Holland Publishing Company, Amsterdam, 1982), Vol. 3, p. 484.
[22] A. Dewald, S. Harissopulos, and P. von Brentano, Z. Phys. A **334**, 163 (1989).
[23] B. Singh, Nucl. Data Sheets **109**, 297 (2008).
[24] G. M. Temmer and N. P. Heydenburg, Phys. Rev. **104**, 967 (1956).
[25] P. H. Stelson and F. K. McGowan, Phys. Rev. **110**, 489 (1958).
[26] S. Landsberger, R. Lecomte, P. Paradis, and S. Monaro, Phys. Rev. C **21**, 588 (1980).
[27] J. H. Hirata, S. Salém-Vasconcelos, M. J. Bechara, L. C. Gomes, and O. Dietzsch, Phys. Rev. C **57**, 76 (1998).
[28] D. Abriola and A. A. Sonzogni, Nucl. Data Sheets **107**, 2423 (2006).
[29] D. Abriola and A. A. Sonzogni, Nucl. Data Sheets **109**, 2501 (2008).
[30] B. Singh and Z. Hu, Nucl. Data Sheets **98**, 335 (2003).
[31] T. Konstantinopoulos, S. F. Ashley, M. Axiotis, A. Spyrou, S. Harissopulos, A. Dewald, J. Litzinger, O. Möller, C. Müller-Gatterman, P. Petkov, D. R. Napoli, N. Marginean, G. de Angelis, C. A. Ur, D. Bazzacco, E. Farnea, S. M. Lenzi, R. Vlastou, and D. Balabanski, Phys. Rev. C **93**, 014320 (2016).
[32] N. Boelaert, A. Dewald, C. Fransen, J. Jolie, A. Linnemann, B. Melon, O. Möller, N. Smirnova, and K. Heyde, Phys. Rev. C **75**, 054311 (2007).
[33] A. Ekström, J. Cederkäll, C. Fahlander, M. Hjorth-Jensen, F. Ames, P. A. Butler, T. Davinson, J. Eberth, F. Fincke, A. Görgen, M. Górska, D. Habs, A. M. Hurst, M. Huyse, O. Ivanov, J. Iwanicki, O. Kester, U. Köster, B. A. Marsh, J. Mierzejewski, P. Reiter, H. Scheit, D. Schwalm, S. Siem, G. Sletten, I. Stefanescu, G. M. Tveten, J. Van de Walle, P. Van Duppen, D. Voulot, N. Warr, D. Weisshaar, F. Wenander, and M. Zielińska, Phys. Rev. Lett. **101**, 012502 (2008).
[34] T. Bäck, C. Qi, F. Ghazi Moradi, B. Cederwall, A. Johnson, R. Liotta, R. Wyss, H. Al-Azri, D. Bloor, T. Brock, R. Wadsworth, T. Grahn, P. T. Greenlees, K. Hauschild, A. Herzan, U. Jacobsson, P. M. Jones, R. Julin, S. Juutinen, S. Ketelhut, M. Leino, A. Lopez-Martens, P. Nieminen, P. Peura, P. Rahkila, S. Rinta-Antila, P. Ruotsalainen, M. Sandzelius, J. Sarén, C. Scholey, J. Sorri, J. Uusitalo, S. Go, E. Ideguchi, D. M. Cullen, M. G. Procter, T. Braunroth, A. Dewald, C. Fransen, M. Hackstein, J. Litzinger, and W. Rother, Phys. Rev. C **84**, 041306(R) (2011).
[35] R. Budaca, P. Buganu, M. Chabab, A. Lahbas, and M. Oulne (unpublished).
[36] P. Buganu and R. Budaca, J. Phys. G: Nucl. Part. Phys. **42**, 105106 (2015).
[37] M. Chabab, A. El Batoul, A. Lahbas, and M. Oulne, Nucl. Phys. A **953**, 158 (2016).
[38] A. Petrovici, Phys. Rev. C **85**, 034337 (2012).
[39] B. A. Brown, W. D. M. Rae, E. McDonald, and M. Horoi, NUSHELLX@MSU, http://www.nscl.msu.edu/~brown/resources/resources.html.